Check for updates

AGU ADVANCING EARTH AND SPACE SCIENCE

Geophysical Research Letters

RESEARCH LETTER
10.1029/2023GL102979

Paleogeographic Reconstruction of Precambrian Terranes Reworked by Phanerozoic Orogens: An Example Based on Detrital Zircon REE From Lhasa Terrane in Southern Tibet

Pei-yuan Hu[1], Qing-guo Zhai[1], Peter A. Cawood[2], Roberto F. Weinberg[2], Guo-chun Zhao[3], Yue Tang[1], and Yi-ming Liu[1]

[1]Institute of Geology, Chinese Academy of Geological Sciences, Beijing, China, [2]School of Earth, Atmosphere & Environment, Monash University, Melbourne, VIC, Australia, [3]Department of Earth Sciences, University of Hong Kong, Hong Kong, China

Key Points:

- Zircon rare earth element (REE) abundances reflect the composition of, and the conditions that generated, the parental melts
- Trends in detrital zircon REE effectively preserve a crustal evolution history and provide a new approach for paleogeographic reconstruction
- The Lhasa terrane in the southern Tibet had an African affinity in the Rodinia-Gondwana supercontinent cycles

Supporting Information:

Supporting Information may be found in the online version of this article.

Correspondence to:

P.-y. Hu,
azure_jlu@126.com

Citation:

Hu, P.-y., Zhai, Q.-g., Cawood, P. A., Weinberg, R. F., Zhao, G.-c., Tang, Y., & Liu, Y.-m. (2023). Paleogeographic reconstruction of Precambrian terranes reworked by Phanerozoic orogens: An example based on detrital zircon REE from Lhasa terrane in southern Tibet. *Geophysical Research Letters*, *50*, e2023GL102979. https://doi.org/10.1029/2023GL102979

Received 24 JAN 2023
Accepted 20 FEB 2023

Author Contributions:

Conceptualization: Pei-yuan Hu
Funding acquisition: Pei-yuan Hu, Qing-guo Zhai, Peter A. Cawood
Investigation: Pei-yuan Hu, Qing-guo Zhai, Yue Tang, Yi-ming Liu
Project Administration: Qing-guo Zhai, Guo-chun Zhao
Software: Yue Tang, Yi-ming Liu
Supervision: Qing-guo Zhai, Peter A. Cawood, Guo-chun Zhao
Writing – original draft: Pei-yuan Hu

© 2023. The Authors.
This is an open access article under the terms of the Creative Commons Attribution License, which permits use, distribution and reproduction in any medium, provided the original work is properly cited.

Abstract Paleogeographic reconstruction of Precambrian terranes reworked by Phanerozoic orogens (e.g., the Tibetan Plateau) results in complex lithotectonic relations due to intracrustal reworking by tectonothermal events. Detrital zircon rare earth element (REE) databases at global (global major river sands) and regional (the Gangdese Mountains, southern Tibet) scales reveal trends in $\overline{LREE_N}/\overline{HREE_N}$ and Eu/Eu* that effectively record the crustal evolution of the source, including crustal thickness and redox state of the magma that generated the zircons. Regional comparisons of these chemical markers provide a new approach for paleogeographic reconstructions that we apply to study the origin of the Lhasa terrane, southern Tibet. Using Precambrian to early Paleozoic sedimentary and igneous rocks in the Lhasa terrane and compiling detrital zircon analyses from the northern margin of Gondwana, we show that the Lhasa terrane had an African affinity in the Rodinia–Gondwana supercontinent cycles (ca. 1.4–0.4 Ga).

Plain Language Summary Constraining the paleogeographic positions and affinities of continental fragments plays a crucial role in validating the concept of the supercontinent cycle. However, tracking the evolving paleogeographic position of these fragments, especially for those of Precambrian age, has proven difficult. We explore the potential for solving this problem by using detrital zircon rare earth element (REE) abundances, which are controlled by the magma source depth, protolith type, oxygen fugacity, and magmatic water content of parental melts. We reveal correlations between detrital zircon REE abundances and crustal evolution in different tectonic settings based on global and regional detrital zircon databases. We subsequently demonstrate how detrital zircon REE abundances show that the Lhasa terrane in the southern Tibet is a fragment derived from Africa. Our study provides a new perspective on the paleogeographic reconstruction of continental fragments through Earth's history and thus has important implications for supercontinent research.

1. Introduction

Constraining the paleogeographic positions and affinities of continental fragments plays a crucial role in validating the concept of the supercontinent cycle (Nance et al., 2014). However, the paleogeographic record of a continental fragment is a complex amalgam of magmatic, deformational, metamorphic, and sedimentary events (e.g., Cawood et al., 2022; Zhao et al., 2018) that results from the reworking of older continental fragments in younger orogenic belts (e.g., the Tibetan Plateau; Kapp & DeCelles, 2019). Tracking the evolving paleogeographic position of these fragments, especially for those of Precambrian age, has proven difficult. This is due in part to the lack of fossils and associated faunal affinities between fragments and the overprinting of possible paleomagnetic and stratigraphic records by younger orogenic systems. Previous studies have tried to solve this problem by detrital zircon U-Pb dating and Hf-isotope analyses (e.g., Hu, Zhai, Zhao, et al., 2018). However, the applicability of such data sets to link the basin in which the detrital zircons accumulated to a specific source from which they were derived is dependent on the uniqueness of the latter; for example, spatially separated sources displaying similar records of tectono-magmatic events limit the ability to link basin to a specific source (e.g., Guo et al., 2017; Zhu et al., 2011), unless other unique criteria can be established.

Over the last few decades, there has been an astounding growth in detrital zircon analysis, which has increasingly extended beyond U-Pb and Hf isotopic data to include trace and rare earth elements (REE) (e.g., Zhu et al., 2020). Zircon REE compositions are an important additional data set because they reflect the composition of, and the

Writing – review & editing: Peter A. Cawood, Roberto F. Weinberg, Guo-chun Zhao

conditions that generated, the parental melts (Chapman et al., 2016; Rubatto et al., 2013) and provide insight into the evolutionary history of the continental crust (McKenzie et al., 2018; Tang et al., 2020; Zhu, Campbell, et al., 2022). This paper reveals correlations between detrital zircon REE abundances and crustal evolution in different tectonic settings based on global and regional detrital zircon databases. From this, we demonstrate how detrital zircon REE abundances can be used to link basin and source by a case study of tracking the origin of the Lhasa terrane, southern Tibet, which is a typical Precambrian terrane reworked by Phanerozoic orogens (Guo et al., 2017; Hu, Zhai, Zhao, et al., 2018). Our study provides a new perspective on the paleogeographic reconstruction of continental fragments through Earth's history.

2. Rationale

Felsic igneous rocks constitute the dominant source of detrital zircons. Zircons sequester heavy (H) REEs relative to light (L) REEs from the parental melt (Hoskin & Schaltegger, 2003). To limit the influence of different degrees of compatibilities of REEs in zircon, we use $\overline{\mathrm{LREE_N}}/\overline{\mathrm{HREE_N}}$ as a proxy to estimate the zircon REE differentiation degree. N denotes normalized to the average REE abundances of granitic zircons reported by Belousova et al. (2002). $\overline{\mathrm{LREE_N}}$ and $\overline{\mathrm{HREE_N}}$ are the average normalized abundances of LREE and HREE, respectively. Moreover, unlike other REEs, which are trivalent (except Ce), Eu exists as both Eu^{2+} and Eu^{3+} in most magmatic systems. Eu^{2+} is significantly more incompatible than Eu^{3+} in zircon, and the variation of Eu concentration in zircon with respect to its neighboring REEs (Sm and Gd) is commonly measured as an Eu anomaly (Eu/Eu*; chondrite normalized $\mathrm{Eu}/\sqrt{\mathrm{Sm} \times \mathrm{Gd}}$) (Tang et al., 2020). Generally, $\overline{\mathrm{LREE_N}}/\overline{\mathrm{HREE_N}}$ and Eu/Eu* of zircons from felsic igneous rocks are controlled by the following factors of the parental melt:

1. Magma source depth. Eu^{2+} is geochemically similar to Sr^{2+} and Ca^{2+} and thus strongly partitions into plagioclase (Ren, 2004). In a deep magma source, anatexis or fractional crystallization takes place at high pressures, which suppresses plagioclase crystallization (Tang et al., 2020). HREEs are much more compatible than LREEs in garnet, which is more stable in deeper magma sources (Rubatto et al., 2013). Therefore, deep magma sources would lead to high Eu abundances and LREE/HREE ratios in the melt, which in turn result in high Eu/Eu* and $\overline{\mathrm{LREE_N}}/\overline{\mathrm{HREE_N}}$ in the zircon.
2. Protolith type. Based on the protolith type, felsic igneous rocks can be divided into two end-members: I- (igneous protoliths) and S- (sedimentary protoliths) types. Generally, S-type felsic igneous rocks are derived from the Eu-depleted upper continental crust (Rudnick & Gao, 2014). Whole-rock Eu/Eu* is likely inherited from protoliths and influences zircon Eu/Eu* to some extent (Tang et al., 2020). Moreover, experimental data of crustal rocks have revealed that the lower pressure limit of garnet stability is lower in sedimentary protoliths (~0.5 GPa) than in igneous protoliths (~1.2 GPa) (Palin et al., 2016; Qian & Hermann, 2013; Wang et al., 2012), implying that zircons from S-type felsic igneous rocks would display higher $\overline{\mathrm{LREE_N}}/\overline{\mathrm{HREE_N}}$ than the I-type counterparts with other conditions unchanged. Finally, the REE abundances of zircons can be influenced by their cogenetic minerals. Garnet, as a cogenetic phase of zircon, is rather uncommon in I-type felsic igneous rocks. By contrast, garnets appear in some strongly peraluminous S-type felsic igneous rocks (e.g., leucogranite) (e.g., Ding et al., 2021). In this case, most HREEs are sequestered in the garnets, resulting in high zircon $\overline{\mathrm{LREE_N}}/\overline{\mathrm{HREE_N}}$ (Rubatto et al., 2013). In summary, an increased proportion of zircon from S-type felsic igneous rock in detrital zircons generally leads to higher $\overline{\mathrm{LREE_N}}/\overline{\mathrm{HREE_N}}$ and lower Eu/Eu*.
3. Oxygen fugacity. Reduced conditions can increase Eu^{2+}/Eu^{3+} and Fe^{2+}/Fe^{3+} ratios in the melt, whereas oxidized conditions have the opposite effects. High Eu^{2+}/Eu^{3+} leads to low zircon Eu/Eu*. High Fe^{2+}/Fe^{3+} is conducive to garnet growth, which preferentially sequesters Fe^{2+} over Fe^{3+} from the melt (Tang et al., 2018), leading to high zircon $\overline{\mathrm{LREE_N}}/\overline{\mathrm{HREE_N}}$.
4. Magmatic water content. The currently available data do not suggest a strong correlation between magmatic water content and the crystallization pressure of garnet (Hirschmann, 2006). However, higher water contents increase plagioclase melting and suppress plagioclase crystallization (Triantafyllou et al., 2023), resulting in higher whole-rock Eu and positive zircon Eu/Eu* (Dilles et al., 2015).

The influence of the factors outlined above varies through the tectonic evolution of an orogen. A high proportion of zircon from S-type felsic igneous rock in detrital zircons (>10%) requires a post-collision setting after the rapid erosion of the high mountains that formed during continent-continent collisions (Zhu et al., 2020). Oceanic subduction and syn-collision tectonic settings result in relatively low production of S-type felsic igneous rock (<10% in detrital zircon proportion; Zhu et al., 2020). Moreover, the oxygen fugacity and magmatic water

19448007, 2023, 5, Downloaded from https://agupubs.onlinelibrary.wiley.com/doi/10.1029/2023GL102979 by University of Hong Kong, Wiley Online Library on [18/09/2023]. See the Terms and Conditions (https://onlinelibrary.wiley.com/terms-and-conditions) on Wiley Online Library for rules of use; OA articles are governed by the applicable Creative Commons License

content are stably high in continental arcs because of continuous oceanic subduction (Zhao et al., 2022). By contrast, the oxygen fugacity and magmatic water content are more complicated in continent-continent collision settings (Wang et al., 2018). With the cessation of oceanic subduction, the oxygen fugacity and magmatic water content tend to be lower. However, they can be elevated by some local collision-related geological processes, such as the subduction of high-oxygen sedimentary rocks, dehydration of subducted continental crust, or injection of mantle-derived ultrapotassic melts (Wang et al., 2018). Given these reasons, we reach the following two hypotheses:

1. In oceanic subduction settings, the zircon REE abundances are mainly controlled by the magma source depth of melt because of the low proportion of zircon from S-type felsic igneous rock and stably high oxygen fugacity and magmatic water content. In this case, the zircon $\overline{LREE_N}/\overline{HREE_N}$ and Eu/Eu* are coupled and correlate with the magma source depth, whose average has been interpreted to reflect crustal thickness (Chapman et al., 2015; Tang et al., 2020).
2. In continent-continent collision settings, although magma source depth is still an important controlling factor, as a result of the variation of oxygen fugacity, magmatic water content, and proportion of zircon from S-type felsic igneous rock (Wang et al., 2018; Zhu et al., 2020), zircon $\overline{LREE_N}/\overline{HREE_N}$ and Eu/Eu* tend to be decoupled.

3. Results: Correlation Between Detrital Zircon REE Abundances and Crustal Evolution

We evaluate these hypotheses by two typical detrital zircon databases of regional and global scales: the Gangdese Mountains in southern Tibet (Tang et al., 2020) (Table S1 in Supporting Information S1) and the global major river sands (Zhu et al., 2020) (Table S2 in Supporting Information S1). The detrital zircon $\overline{LREE_N}/\overline{HREE_N}$ and Eu/Eu* data are plotted as binned averages calculated by both mean and median methods (Figures 1a–1d). To ensure statistical accuracy, the relationships between trends in zircon $\overline{LREE_N}/\overline{HREE_N}$ and Eu/Eu* are classified into three types: coupled (both mean and median trends are coupled), partly decoupled (either mean or median trends are decoupled), and decoupled (both mean and median trends are decoupled).

On a regional scale, these hypotheses are consistent with data from the well-studied Gangdese Mountains in southern Tibet, a typical modern orogenic belt (Hao et al., 2019; Tang et al., 2020; Zhao et al., 2021; Zhu et al., 2017). We exclude zircon analyses with ages >90 Ma to eliminate the influence of the Qiangtang-Lhasa collision and subsequent post-collision events (Wang et al., 2014). Recent studies further constrained the timing of the initial collision between India and Asia to ca. 55 Ma, and indicated that oceanic subduction terminated at ca. 45 Ma as a result of slab breakoff (Hu et al., 2016; Zhu et al., 2015). In the stage with active oceanic subduction (ca. 90–45 Ma), the means and medians of zircon $\overline{LREE_N}/\overline{HREE_N}$ and Eu/Eu* are mostly coupled (except for the period from ca. 72.5 to 67.5 Ma) and correlate with the crustal thickness (Tang et al., 2020) (Figures 1a and 1b). The partly decoupled $\overline{LREE_N}/\overline{HREE_N}$ period from ca. 72.5 to 67.5 Ma is possibly due to the rising asthenosphere triggered by coeval roll-back of oceanic slab (Zhu, Wang, et al., 2022) that modified the redox conditions or water content of the magmatic system. This roll-back event is further supported by the subsequent crustal thinning process from ca. 67.5 to 57.5 Ma (Figure 1e). Moreover, the $\overline{LREE_N}/\overline{HREE_N}$ and Eu/Eu* values become mostly decoupled or partly decoupled in the continent-continent collision stage (ca. 45–0 Ma). Although the data in the time bins of 32.5 Ma and 27.5 Ma may be unreliable because of the relatively small sample size (<20), their neighboring time bins with ≥20 data (42.5, 22.5, 17.5, and 12.5 Ma) are all decoupled or partly decoupled. Notably, the crust thinned by about 20 km during the ca. 27–15 Ma period (Figure 1e), which is interpreted to be a result of the foundering of subducted continental plate in previous studies and supported by coeval fault activation and the formation of the Kailas basin and the ca. 24–23 Ma Konglong A-type magmatism in the Gangdese Mountains (e.g., DeCelles et al., 2011; Hao et al., 2019). This process is expressed by decoupled $\overline{LREE_N}/\overline{HREE_N}$ and Eu/Eu*, possibly because of the integrated effect of thinned crust decreasing $\overline{LREE_N}/\overline{HREE_N}$ and regional oxidation events (e.g., injection of upwelling mantle-derived ultrapotassic melts; Wang et al., 2018) causing an increase in Eu/Eu*.

At a global scale, these hypotheses are supported by the detrital zircon database from major river sands worldwide (Zhu et al., 2020). The periods of extensive high mountain formation in Earth's history are represented by the age peaks of low-Lu zircon (Lu < 10 ppm and Lu/Dy < 0.35), which predominantly comes from the deep roots

19448007, 2023, 5, Downloaded from https://agupubs.onlinelibrary.wiley.com/doi/10.1029/2023GL102979 by University of Hong Kong, Wiley Online Library on [18/09/2023]. See the Terms and Conditions (https://onlinelibrary.wiley.com/terms-and-conditions) on Wiley Online Library for rules of use; OA articles are governed by the applicable Creative Commons License

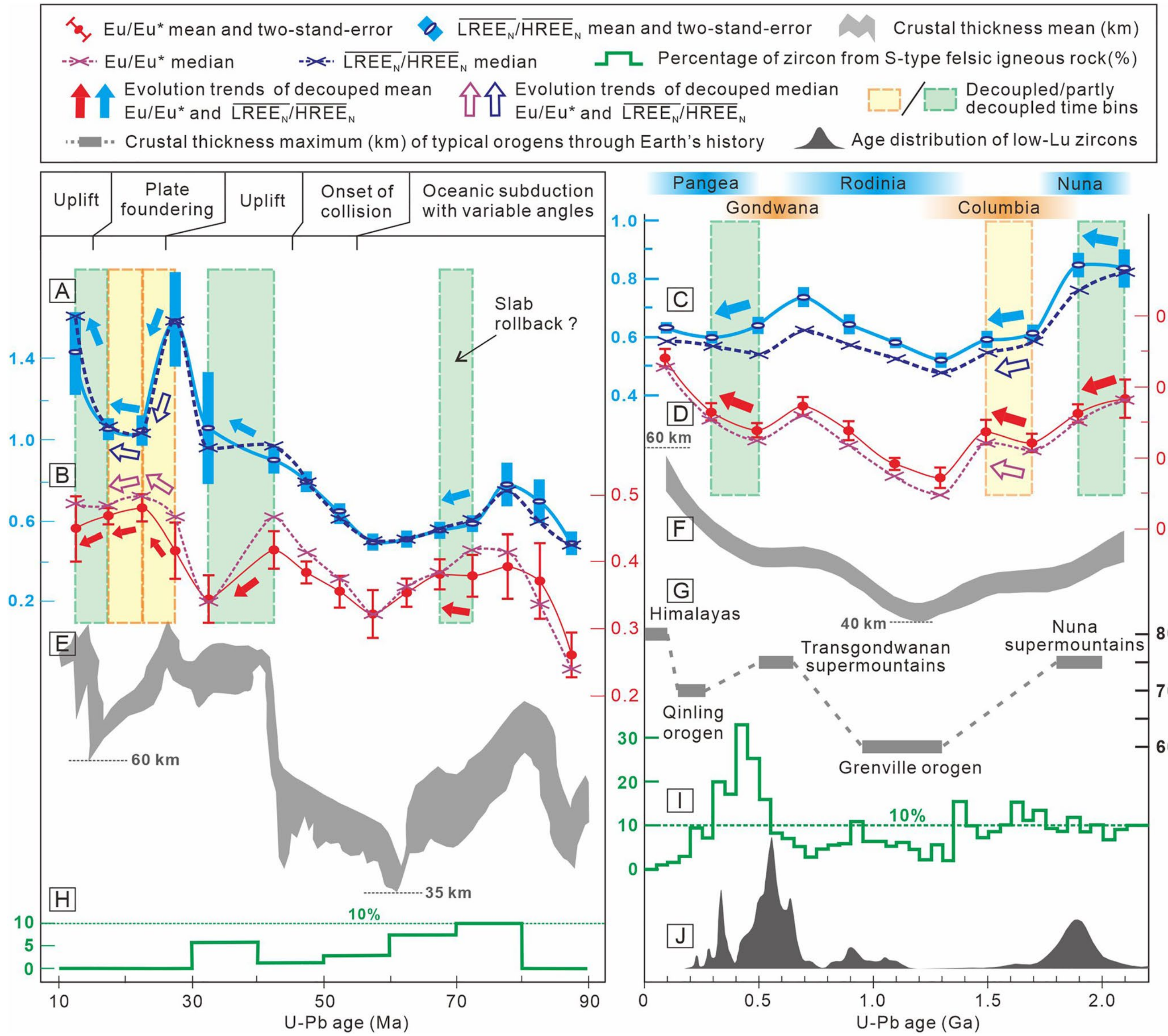

Figure 1. Detrital zircon $\overline{\mathrm{LREE}_N}/\overline{\mathrm{HREE}_N}$ and Eu/Eu* distributions for the Gangdese Mountains in southern Tibet (a–b) (Tang et al., 2020) and the global major river sands (c–d) (Zhu et al., 2020). The data are available in Table S1 and S2 in Supporting Information S1 and calculated by both mean and median methods. The $\overline{\mathrm{LREE}_N}/\overline{\mathrm{HREE}_N}$ and Eu/Eu* data are plotted as binned averages (bin size: 5 Myr for the Gangdese Mountains and 200 Myr for the global major river sands), with error bars indicating ±2 SEM. This figure also shows the crustal thickness average data of the Gangdese Mountains (e) and global active continental crust (f), which are calculated by whole-rock La/Yb data (Tang et al., 2020) and zircon Eu/Eu* data from I- and A-type felsic igneous rocks (Tang et al., 2021), respectively. The maximum crustal thickness of the Himalayas, Qinling orogen, Transgondwanan supermountains, Grenville orogen, and Nuna supermountains (g) (Brudner et al., 2022; Hu et al., 2017, 2020; Zhu, Campbell, et al., 2022; Zhu et al., 2017) are also shown for comparison. The percentage of S-type zircon in every time bin (h and i) and the age distribution of low-Lu zircons (j) (calculated by Isoplot/Ex ver. 3.0; Ludwig, 2003) are also compared. The S-type zircons are distinguished by their relatively high P contents (>750 ppm; Burnham & Berry, 2017). The time windows of Pangea, Gondwana, Rodinia, Columbia, and Nuna are from Wang et al. (2021). The data filtering rules are: (1) The $^{207}Pb/^{206}Pb$ ages were used for those older than 1,000 Ma, and $^{206}Pb/^{238}U$ ages were used for younger zircons. (2) Analyses with Th/U < 0.1 (except low-Lu zircons) were excluded to eliminate metamorphic zircons. (3) Analyses with discordance >10% or La >1 ppm were excluded to ensure age accuracy and eliminate data compromised by inclusions (Hoskin & Schaltegger, 2003). (4) The highest 10% and lowest 10% ratios within each bin were removed to reduce scatter when calculating means. (5) The bins with ≤10 data points are not shown because of low reliability.

that underlie ultrahigh Himalayan-type mountains (Zhu, Campbell, et al., 2022). As shown in Figures 1c and 1d, zircon $\overline{\mathrm{LREE}_N}/\overline{\mathrm{HREE}_N}$ and Eu/Eu* are decoupled or partly decoupled at ca. 2.0 Ga, 1.6 Ga, and 0.4 Ga, roughly coeval with the age peaks defined by low-Lu zircons (Figure 1j) or the periods with high production of zircon from S-type felsic igneous rock (>10%) (Figure 1i), probably because of the extensive syn- or post-collision events associated with the assembly of Nuna, Columbia, and Gondwana. The decoupled $\overline{\mathrm{LREE}_N}/\overline{\mathrm{HREE}_N}$ and

19448007, 2023, 5, Downloaded from https://agupubs.onlinelibrary.wiley.com/doi/10.1029/2023GL102979 by University of Hong Kong, Wiley Online Library on [18/09/2023]. See the Terms and Conditions (https://onlinelibrary.wiley.com/terms-and-conditions) on Wiley Online Library for rules of use; OA articles are governed by the applicable Creative Commons License

Eu/Eu* trends can be further divided into two types. The first type is characterized by increased $\overline{LREE_N}/\overline{HREE_N}$ and decreased Eu/Eu*, which can be explained by the increased proportion of zircon from S-type felsic igneous rock or the reduced conditions in collision-related settings. The second type displays decreased $\overline{LREE_N}/\overline{HREE_N}$ and increased Eu/Eu* and may be related to oxidation events resulted from continental subduction during supercontinent assembly (e.g., subduction of high-oxygen sedimentary rocks; Wang et al., 2018). In contrast, Rodinia (1.3–0.7 Ga) is a period of coupled zircon $\overline{LREE_N}/\overline{HREE_N}$ and Eu/Eu*, which positively correlates with the global average crustal thickness (Figures 1c–1f). A possible reason is that the Rodinian margins were dominantly Andean in style (low production of both S-type and low-Lu zircons; Figures 1i and 1j) (Spencer et al., 2013; Zhu et al., 2020) and the core of the Rodinian continental configuration was mostly inherited from Columbia (Cawood & Hawkesworth, 2014; Cawood et al., 2016). This reason is also supported by the lower maximum crustal thickness (~60 km) of the Grenville orogen than those of the typical orogens within other supercontinents (Pangea, ~70 km; Gondwana, ~75 km; Nuna, ~75 km) and the Himalayas (~90 km) (Brudner et al., 2022; Hu et al., 2017, 2020; Zhu, Campbell, et al., 2022) (Figure 1g), as mountain chains generated by continent-continent collisions are generally taller and larger in volume than those generated by subduction-related processes (Campbell & Squire, 2010; Zhu, Campbell, et al., 2022).

4. The Lhasa Terrane Originates From Africa as Constrained by Detrital Zircon REE Comparisons

The above results reveal that trends in zircon $\overline{LREE_N}/\overline{HREE_N}$ and Eu/Eu* effectively preserve a crustal evolution history. If two terranes were adjacent, they should share a similar crustal evolution history. Hence, the comparative study of detrital zircon REE data provides a new approach for unraveling paleogeographic reconstructions of older, Precambrian terranes reworked by younger, Phanerozoic orogens. The Lhasa terrane provides an ideal case study to evaluate this new approach of paleogeographic reconstruction. Extensive Precambrian basement rocks have been identified in the terrane (e.g., Dong et al., 2022; Hu, Zhai, Zhao, et al., 2018, Hu, Zhai, Wang, et al., 2018; Wu et al., 2016), and the pre-Permian paleomagnetic and stratigraphic records in this terrane were modified by Mesozoic-Cenozoic tectonic events that extend across much of the Tibetan Plateau (Kapp & DeCelles, 2019). There is a broad consensus that the Lhasa terrane was derived from the northern margin of Gondwana (African, Indian, or Australian Gondwana) (Cawood et al., 2021; Guo et al., 2017; Hu, Zhai, Zhao, et al., 2018; Zhu et al., 2011), where previous studies have reported abundant detrital zircon data for comparison. We report in situ U-Pb age, Hf-isotope, and REE data for 863 zircons from the Precambrian to early Paleozoic sedimentary and felsic igneous rocks in the Lhasa terrane (Text S1 in Supporting Information S1 for detailed sample descriptions, analytical methods, and results) and integrate this data with >18,000 detrital zircon analyses from 55 localities across northern Gondwana that were reported in previous studies (Figures 2 and 3; Tables S3–S10 in Supporting Information S1).

Pre-1.4 Ga zircons are rare in the data analyzed or collected in this study (Figures S6 and S7 in Supporting Information S1), so our integrated analysis of detrital zircon REE data focuses on the time range of 1.4–0 Ga. Some data from the African, Indian and Australian continents include sediments deposited during the Mesozoic-Cenozoic when the Lhasa terrane had drifted away from Gondwana (Zhu et al., 2010). These data are not directly related to the Lhasa terrane, but they can be used to reconstruct the crustal evolution histories of the continents in the northern Gondwana and indirectly constrain the paleogeographic affinity of the Lhasa terrane. This is because African, Indian, and Australian continents are mostly separated by ocean basins or orogenic belts in the time range of 1.4–0 Ga, which prevented extensive exchange of detrital zircons from different continents (Merdith et al., 2017) and indicates a predominant local source for the Mesozoic-Cenozoic sediments in these continents. For example, in the period of Gondwanan supercontinent amalgamation, although these continents were temporarily connected, they were separated by major collisional orogens, such as the Kuunga-Pinjarra and East Africa orogens (Figure 2b). For a similar reason, previous studies in India and Africa have revealed that the chemical and isotopic compositions of detrital zircons from young strata effectively preserve an ancient crustal evolution history (Iizuka et al., 2013; McKenzie et al., 2018).

Moreover, after the Lhasa terrane drifted away from northern Gondwana, it was probably a microcontinent isolated in the Paleo-Tethyan Ocean basin before the Cretaceous Lhasa-Qiangtang and Cenozoic Himalaya-Lhasa collisions (Hu et al., 2020; Zhu et al., 2010). However, the post-Cretaceous sedimentary rocks in the Lhasa terrane may be unreliable as a result of the mixing of detrital zircons from the South Qiangtang terrane or

19448007, 2023, 5, Downloaded from https://agupubs.onlinelibrary.wiley.com/doi/10.1029/2023GL102979 by University of Hong Kong, Wiley Online Library on [18/09/2023]. See the Terms and Conditions (https://onlinelibrary.wiley.com/terms-and-conditions) on Wiley Online Library for rules of use; OA articles are governed by the applicable Creative Commons License

19448007, 2023, 5, Downloaded from https://agupubs.onlinelibrary.wiley.com/doi/10.1029/2023GL102979 by University of Hong Kong, Wiley Online Library on [18/09/2023]. See the Terms and Conditions (https://onlinelibrary.wiley.com/terms-and-conditions) on Wiley Online Library for rules of use; OA articles are governed by the applicable Creative Commons License

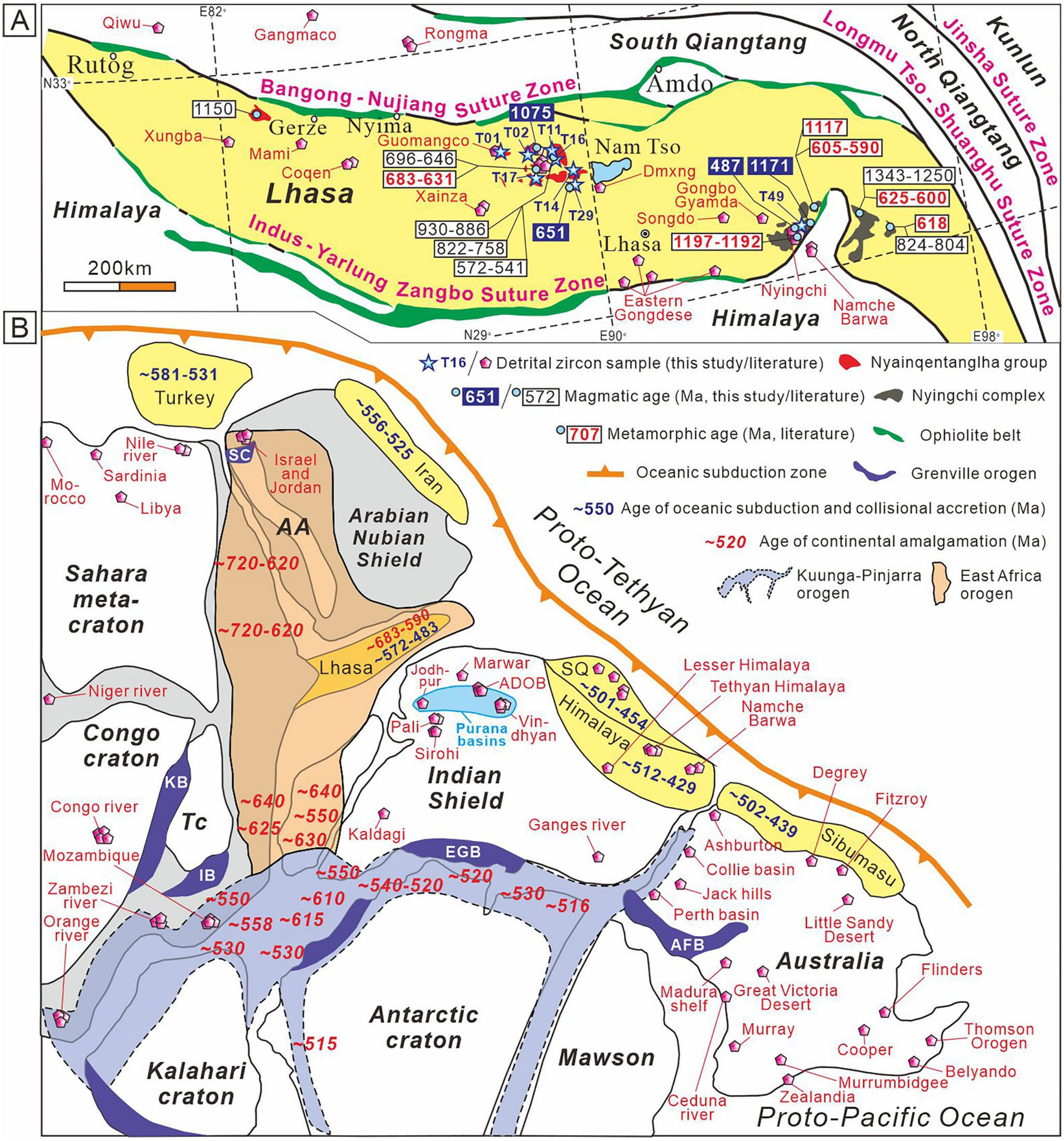

Figure 2. (a) Tectonic framework of the central Tibetan Plateau (modified from Zhu et al., 2011), showing the distribution of Precambrian rocks, magmatic ages, and sampling locations. (b) Gondwana reconstruction showing the locations and times of major orogens (modified from Hu, Zhai, Wang, et al., 2018). The sources of the detrital zircon data and magmatic-metamorphic ages are given in Tables S3 and S4 in Supporting Information S1, respectively. ADOB = Aravalli-Delhi Orogenic Belt; EGB = Eastern Ghats Belt; AFB = Albany-Fraser Belt; AA = Afif-Abas terrane; TC = Tanzania craton; SC = Sa'al Complex; KB = Kibaran Belt; IB = Irumide Belt.

Himalaya area, so we excluded these data, except those from modern river sands in the Gangdese belt, which have been interpreted to dominantly have a local source (Tang et al., 2020).

In the Rodinian supercontinent cycle (1.3–0.7 Ga), global active continental margins were dominantly Andean in style (Spencer et al., 2013; Zhu et al., 2020). The Australian zircon $\overline{LREE_N}/\overline{HREE_N}$ and Eu/Eu* values show

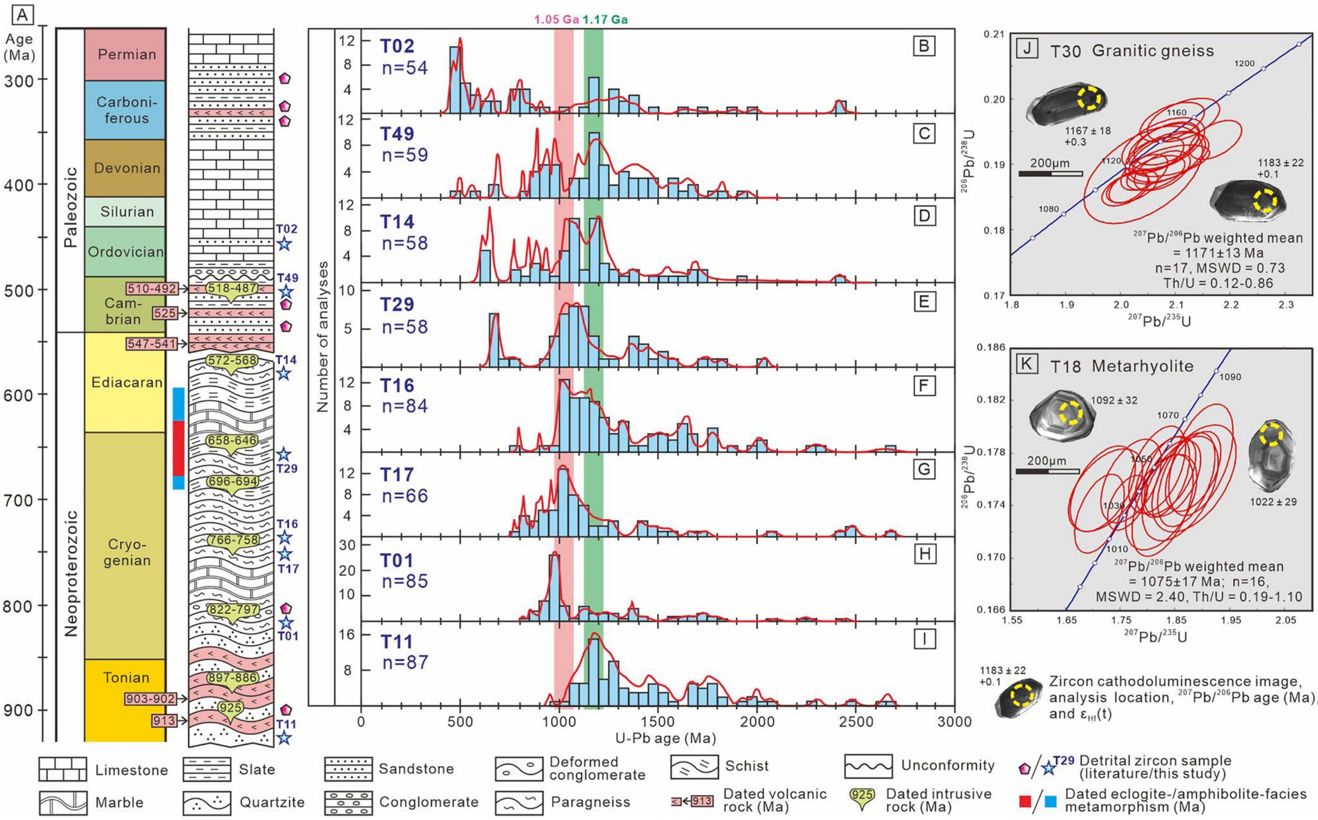

Figure 3. Simplified stratum column of the Lhasa terrane (modified from BGMR, 1993) (a), histograms for the U-Pb ages of detrital zircons samples (b)–(i) and concordia plots for the magmatic samples T30 (j) and T18 (k). The data are available in Tables S5 and S6 in Supporting Information S1. The sample locations are shown in Figure 2A. The data filtering rules are consistent with those of Figure 1. *n* = total number of analyses.

a continuous decrease until 0.9 Ga, whereas India, Africa, and the Lhasa terrane all show decreasing trends from 1.3 to 1.1 Ga and increasing trends from 1.1 to 0.7 Ga, suggesting different variations of crustal thickness (Figures 4m–4p). These data suggests that the Lhasa terrane was not sourced from the Australian section of Rodinia.

During the stage of Gondwanan assembly (0.7–0.5 Ga), Indian zircon $\overline{LREE_N}/\overline{HREE_N}$ and Eu/Eu* were coupled, while the counterparts from the Lhasa terrane, Africa, and Australia were decoupled or partly decoupled (Figures 4m–4p). The likely explanation is that the currently available detrital zircon REE data from India are mostly from its northern and central regions, which were not involved in the collisional belts of the Gondwanan assembly (Wang et al., 2019) (Figure 2b). Notably, the detrital zircons from Africa and the Lhasa terrane show increased $\overline{LREE_N}/\overline{HREE_N}$ and decreased Eu/Eu* (both medians and means) in this stage, whereas the Australian counterparts have decreased mean $\overline{LREE_N}/\overline{HREE_N}$ and increased mean Eu/Eu* as well as consistently increased median $\overline{LREE_N}/\overline{HREE_N}$ and Eu/Eu* (Figures 4m, 4n, and 4p), suggesting different crustal evolution histories.

Overall, our comparative study of detrital zircon REE data in the Rodinia–Gondwana supercontinent cycles (1.4–0.4 Ga) suggests an African affinity for the detrital zircons in the Lhasa terrane. Notably, the $\overline{LREE_N}/\overline{HREE_N}$ and Eu/Eu* trends of detrital zircons from Africa and the Lhasa terrane differ after Gondwanan assembly (Figures 4m and 4n). In the time bin of 500–300 Ma, African zircon Eu/Eu* medians and means increased while the Lhasa counterparts decreased (Figures 4m and 4n), possibly because the Lhasa terrane had drifted away from the northern Gondwana by ca. 300 Ma.

An African affinity for the Lhasa detrital zircons during the Rodinia–Gondwana supercontinent cycles (1.4–0.4 Ga) is consistent with the distribution and character of the magmatic and metamorphic records of Gondwanan assembly. Two types of orogenic systems with different zircon $\varepsilon_{Hf}(t)$ evolution trends have been established by Collins et al. (2011). The range of hafnium isotope signatures for the extensional (external) orogenic systems (e.g.,

19448007, 2023, 5, Downloaded from https://agupubs.onlinelibrary.wiley.com/doi/10.1029/2023GL102979 by University of Hong Kong, Wiley Online Library on [18/09/2023]. See the Terms and Conditions (https://onlinelibrary.wiley.com/terms-and-conditions) on Wiley Online Library for rules of use; OA articles are governed by the applicable Creative Commons License

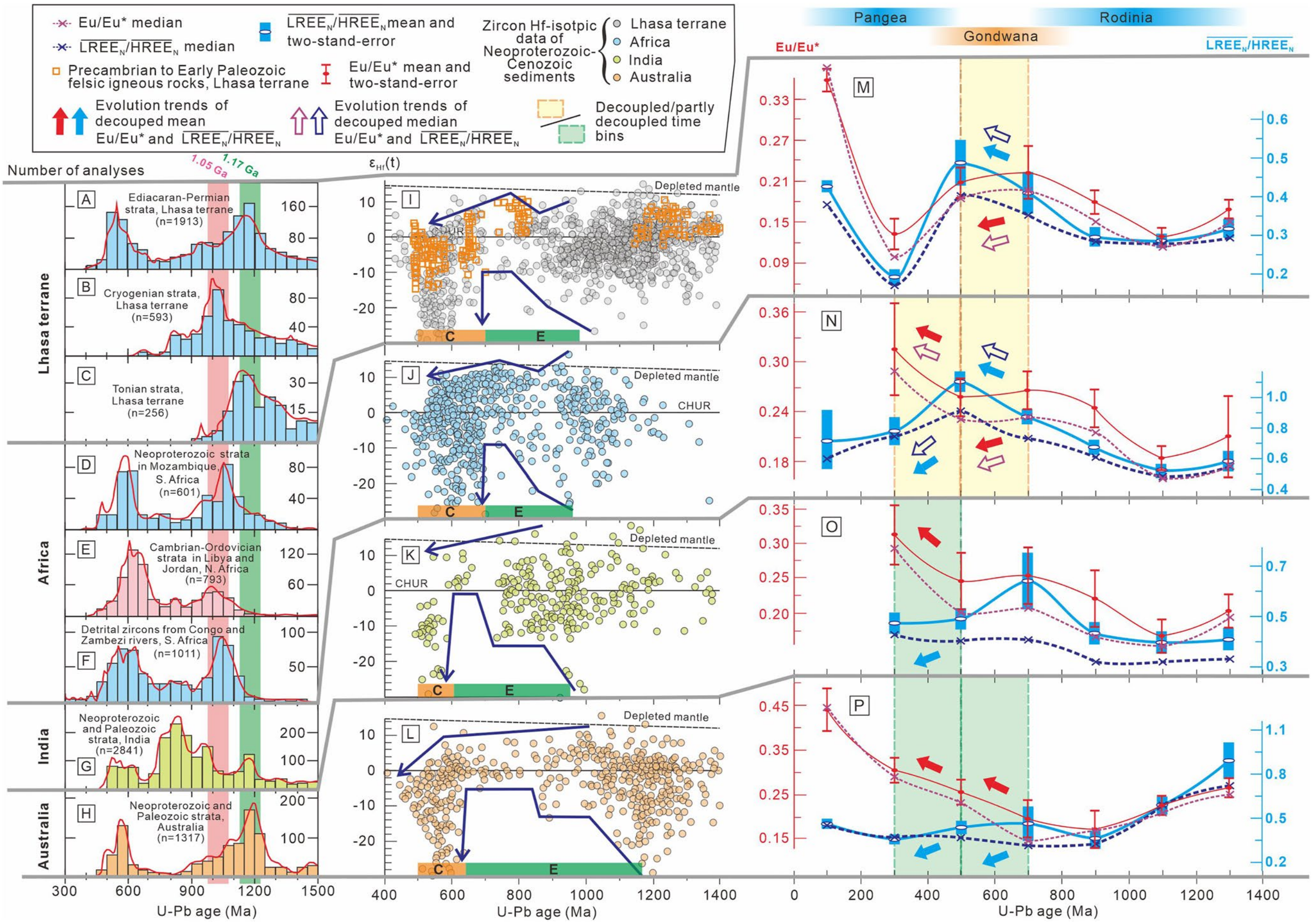

Figure 4. Detrital zircon U-Pb age (A–H), $\varepsilon_{Hf}(t)$ (I–L), $\overline{LREE_N}/\overline{HREE_N}$, and Eu/Eu* (M–P) distributions for the Lhasa terrane and its potential origins in Gondwana. The $\overline{LREE_N}/\overline{HREE_N}$ and Eu/Eu* data are plotted as binned averages (bin size = 200 Myr). The data filtering rules and average calculating method of REE data are consistent with those in Figure 1. The zircon $\varepsilon_{Hf}(t)$ data of Precambrian to Early Paleozoic felsic igneous rocks in the Lhasa terrane were plotted for comparison (analyses with discordance >10% or Th/U < 0.1 ppm were excluded to ensure age accuracy and eliminate metamorphic zircons). The data are available in Tables S5–S9 in Supporting Information S1. The time windows of Pangea, Gondwana, and Rodinia are from Wang et al. (2021). *E* = Extension; *C* = Contraction.

present Asian Pacific rim) narrows and trends toward more radiogenic compositions over timescales to hundreds of millions of years. By contrast, the range of signatures from the contractional (internal) orogenic systems (e.g., present Tibetan plateau) broadens over a similar time scale. The zircon $\varepsilon_{Hf}(t)$ range of the ca. 700–500 Ma felsic igneous rocks in the Lhasa terrane is broader and lower than its ca. 900–700 Ma equivalent (Figure 4i), possibly marking a transition at ca. 700 Ma from an extensional to a contractional orogenic environment. This transition is also supported by the coeval initiation of late Neoproterozoic amphibolite- and granulite-facies metamorphism (683–590 Ma; Figure 3a) in the Lhasa terrane. A coeval transition is identified in Africa, whereas Indian and Australian equivalents are about 100 Ma later (Figures 4j–4l). Additionally, the Ediacaran Proto-Tethyan arc system initiated at the later stage of the Gondwanan assembly (Cawood et al., 2021). Coeval arc-related magmatism occurred in the Lhasa terrane and northern Africa (e.g., Turkey and Iran) but was absent in the outboard terranes along the Indian and Australian Proto-Tethyan margins (e.g., South Qiangtang and Sibumasu) (Hu, Zhai, Wang, et al., 2018) (Figure 2b).

Opinions diverge as to the sources for the sedimentary rocks in the Lhasa terrane. The Tonian and Ediacaran–Permian sedimentary rocks in the terrane display a characteristic age population at ca. 1.17 Ga (Figures 4a and 4c), while their Cryogenian equivalents have a dominant age population of ca. 1.05 Ga (Figure 4b). These late Mesoproterozoic age peaks have been linked to coeval peaks in Australia, India or Africa (Guo et al., 2017; Hu, Zhai, Zhao, et al., 2018; Zhu et al., 2011) (Figures 4d–4h). However, recent studies have identified coeval magmatism (ca. 1,150 Ma, Wu et al., 2016; ca. 1,171 and 1,075 Ma, this study, Figures 3j and 3k) and metamorphism

19448007, 2023, 5, Downloaded from https://agupubs.onlinelibrary.wiley.com/doi/10.1029/2023GL102979 by University of Hong Kong, Wiley Online Library on [18/09/2023]. See the Terms and Conditions (https://onlinelibrary.wiley.com/terms-and-conditions) on Wiley Online Library for rules of use; OA articles are governed by the applicable Creative Commons License

(ca. 1,117 Ma, Lin et al., 2013; ca. 1,197–1,192 Ma, Dong et al., 2022) in the Lhasa terrane. We compared the REE data of ca. 1.2–1.0 Ga detrital zircons from the Lhasa terrane, Africa, India, and Australia and the zircons from two typical late Mesoproterozoic felsic igneous samples from the Lhasa terrane (Figures 3j and 3k; Table S10 in Supporting Information S1; samples T30 and T18). The median $\overline{LREE_N}/\overline{HREE_N}$ and Eu/Eu* of Australia (0.69 and 0.21), India (0.32 and 0.15), and Africa (0.48 and 0.16) are higher than those of the Lhasa terrane (0.27 and 0.11). In contrast, the REE range bracketed by the two late Mesoproterozoic felsic igneous samples T30 (1,171 ± 13 Ma; $\overline{LREE_N}/\overline{HREE_N}$ median = 0.09; Eu/Eu* median = 0.03) and T18 (1,075 ± 17 Ma; $\overline{LREE_N}/\overline{HREE_N}$ median = 0.33; Eu/Eu* median = 0.16) covers the counterparts of ca. 1.2–1.0 Ga detrital zircons from the Lhasa terrane, so we suggest an alternative, local, source for the late Mesoproterozoic detrital zircon age peaks in the Lhasa terrane. This local source can also explains the difference in detrital zircon age distribution between the Lhasa terrane and northern Africa. For example, the Arabian Nubian Shield (ANS) forms one of the largest exposures of Neoproterozoic juvenile continental crust on Earth (Be'eri-Shlevin et al., 2012), probably resulting in the abundant 800–600 Ma detrital zircons in the Neoproterozoic–Paleozoic strata in the ANS and its adjacent areas (e.g., Iran and Turkey; Zoleikhaei et al., 2021, 2022) (Figure 2b), while coeval detrital zircons are relatively uncommon in the Lhasa terrane possibly due to its predominant pre-800 Ma basement rocks (Table S4 in Supporting Information S1).

5. Conclusion and Outlook

Trends in zircon $\overline{LREE_N}/\overline{HREE_N}$ and Eu/Eu* are controlled by the magma source depth, protolith type, oxygen fugacity, and magmatic water content of parental melts, and thus effectively preserve a crustal evolution history and represent a new approach for paleogeographic reconstructions. This approach can be a valuable complement to detrital zircon age and Hf-isotope analyses, helping resolve challenging paleogeographic puzzles. Our comparative study of detrital zircon REE data suggests that the Lhasa terrane probably was attached to northern Africa at least during the Rodinia-Gondwana supercontinent cycles (1.4–0.4 Ga) before it drifted away in the Paleozoic.

Conflict of Interest

The authors declare no conflicts of interest relevant to this study.

Data Availability Statement

Supporting data of this study can be found at https://doi.org/10.6084/m9.figshare.21944846.v1.

Acknowledgments
The authors thank Editor Sarah Feakins for her editorial handling and two anonymous journal reviewers and Xiu-zheng Zhang for their detailed comments that considerably improved the manuscript. The authors thank Carlos E. Ganade for insightful reviews of an early version of this manuscript. This study was supported by the Second Tibetan Plateau Scientific Expedition and Research (STEP) (Grant 2019QZKK0703), the National Key Research and Development Project of China (Grant 2021YFC2901901), the National Science Foundation of China (Grants 41872240 and 42072268), and the Chinese Geological Survey Project (Grant DD20221630). Peter A. Cawood acknowledges support from Australian Research Grant FL160100168.

References

Be'eri-Shlevin, Y., Eyal, M., Eyal, Y., Whitehouse, M. J., & Litvinovsky, B. (2012). The Sa'al volcano-sedimentary complex (Sinai, Egypt): A latest Mesoproterozoic volcanic arc in the northern Arabian Nubian Shield. *Geology*, *40*(5), 403–406. https://doi.org/10.1130/g32788.1

Belousova, E. A., Griffin, W. L., O'Reilly, S. Y., & Fisher, N. I. (2002). Igneous zircon: Trace element composition as an indicator of source rock type. *Contributions to Mineralogy and Petrology*, *143*(5), 602–622. https://doi.org/10.1007/s00410-002-0364-7

BGMR (Bureau of Geology and Mineral Resources of Xizang Autonomous Region). (1993). *Regional geology of Xizang (Tibet) autonomous region*. Geological Publishing House. [in Chinese].

Brudner, A., Jiang, H. H., Chu, X., & Tang, M. (2022). Crustal thickness of the Grenville orogen: A Mesoproterozoic Tibet? *Geology*, *50*(4), 402–406. https://doi.org/10.1130/g49591.1

Burnham, A. D., & Berry, A. J. (2017). Formation of Hadean granites by melting of igneous crust. *Nature Geoscience*, *10*(6), 457–461. https://doi.org/10.1038/ngeo2942

Campbell, I. H., & Squire, R. J. (2010). The mountains that triggered the Late Neoproterozoic increase in oxygen: The Second Great Oxidation Event. *Geochimica et Cosmochimica Acta*, *74*(15), 4187–4206. https://doi.org/10.1016/j.gca.2010.04.064

Cawood, P. A., Chowdhury, P., Mulder, J. A., Hawkesworth, C. J., Capitanio, F. A., Gunawardana, P. M., & Nebel, O. (2022). Secular evolution of continents and the Earth system. *Reviews of Geophysics*, *60*(4), e2022RG000789. https://doi.org/10.1029/2022rg000789

Cawood, P. A., & Hawkesworth, C. J. (2014). Earth's middle age. *Geology*, *42*(6), 503–506. https://doi.org/10.1130/g35402.1

Cawood, P. A., Martin, E. L., Murphy, J. B., & Pisarevsky, S. A. (2021). Gondwana's interlinked peripheral orogens. *Earth and Planetary Science Letters*, *568*, 117057. https://doi.org/10.1016/j.epsl.2021.117057

Cawood, P. A., Strachan, R. A., Pisarevsky, S. A., Gladkochub, D. P., & Murphy, J. B. (2016). Linking collisional and accretionary orogens during Rodinia assembly and breakup: Implications for models of supercontinent cycles. *Earth and Planetary Science Letters*, *449*, 118–126. https://doi.org/10.1016/j.epsl.2016.05.049

Chapman, J. B., Ducea, M. N., DeCelles, P. G., & Profeta, L. (2015). Tracking changes in crustal thickness during orogenic evolution with Sr/Y: An example from the North American Cordillera. *Geology*, *43*(10), 919–922. https://doi.org/10.1130/g36996.1

Chapman, J. B., Gehrels, G. E., Ducea, M. N., Giesler, N., & Pullen, A. (2016). A new method for estimating parent rock trace element concentrations from zircon. *Chemical Geology*, *439*, 59–70. https://doi.org/10.1016/j.chemgeo.2016.06.014

19448007, 2023, 5, Downloaded from https://agupubs.onlinelibrary.wiley.com/doi/10.1029/2023GL102979 by University of Hong Kong, Wiley Online Library on [18/09/2023]. See the Terms and Conditions (https://onlinelibrary.wiley.com/terms-and-conditions) on Wiley Online Library for rules of use; OA articles are governed by the applicable Creative Commons License

19448007, 2023, 5, Downloaded from https://agupubs.onlinelibrary.wiley.com/doi/10.1029/2023GL102979 by University of Hong Kong, Wiley Online Library on [18/09/2023]. See the Terms and Conditions (https://onlinelibrary.wiley.com/terms-and-conditions) on Wiley Online Library for rules of use; OA articles are governed by the applicable Creative Commons License

Collins, W. J., Belousova, E. A., Kemp, A. I. S., & Murphy, J. B. (2011). Two contrasting Phanerozoic orogenic systems revealed by hafnium isotope data. *Nature Geoscience*, *4*(5), 333–337. https://doi.org/10.1038/ngeo1127

DeCelles, P., Kapp, P., Quade, J., & Gehrels, G. (2011). The Oligocene-Miocene Kailas Basin, southwestern Tibet: Record of post-collisional upper plate extension in the Indus-Yarlung suture zone. *The Geological Society of America Bulletin*, *123*(7–8), 1337–1362. https://doi.org/10.1130/b30258.1

Dilles, J. H., Ken, A. J. R., Wooden, J. L., Tosdal, R. M., Koleszar, A., Lee, R. G., & Farmer, L. P. (2015). Zircon compositional evidence for sulfur-degassing from ore-forming arc magmas. *Economic Geology*, *110*(1), 241–251. https://doi.org/10.2113/econgeo.110.1.241

Ding, H. X., Kohn, M. J., & Zhang, Z. M. (2021). Long-lived (ca. 22-24 Myr) partial melts in the eastern Himalaya: Petrochronologic constraints and tectonic implications. *Earth and Planetary Science Letters*, *558*, 116764. https://doi.org/10.1016/j.epsl.2021.116764

Dong, X., Zhang, Z. M., & Tian, Z. L. (2022). Precambrian metamorphic basement of the southern Lhasa terrane, Tibet. *Precambrian Research*, *368*, 106478. https://doi.org/10.1016/j.precamres.2021.106478

Guo, L., Zhang, H. F., Harris, N., Xu, W. C., & Pan, F. B. (2017). Detrital zircon U-Pb geochronology, trace-element and Hf isotope geochemistry of the metasedimentary rocks in the Eastern Himalayan syntaxis: Tectonic and paleogeographic implications. *Gondwana Research*, *41*, 207–221. https://doi.org/10.1016/j.gr.2015.07.013

Hao, L. L., Wang, Q., Wyman, D. A., Ma, L., Wang, J., Xia, X. P., & Ou, Q. (2019). First identification of postcollisional A-type magmatism in the Himalayan-Tibetan orogen. *Geology*, *47*(2), 187–190. https://doi.org/10.1130/g45526.1

Hirschmann, M. M. (2006). Water, melting, and the deep Earth H_2O cycle. *Annual Review of Earth and Planetary Sciences*, *34*(1), 629–653. https://doi.org/10.1146/annurev.earth.34.031405.125211

Hoskin, P. W. O., & Schaltegger, U. (2003). The composition of zircon and igneous and metamorphic petrogenesis. *Reviews in Mineralogy and Geochemistry*, *53*(1), 27–62. https://doi.org/10.2113/0530027

Hu, F. Y., Ducea, M. N., Liu, S. W., & Chapman, J. B. (2017). Quantifying crustal thickness in continental collisional belts: Global perspective and a geologic application. *Scientific Reports*, *7*(1), 7058. https://doi.org/10.1038/s41598-017-07849-7

Hu, F. Y., Wu, F. Y., Chapman, J. B., Ducea, M. N., Ji, W. Q., & Liu, S. W. (2020). Quantitatively tracking the elevation of the Tibetan Plateau since the Cretaceous: Insights from whole-rock Sr/Y and La/Yb ratios. *Geophysical Research Letters*, *47*(15), e2020GL089202. https://doi.org/10.1029/2020gl089202

Hu, P. Y., Zhai, Q. G., Wang, J., Tang, Y., Wang, H. T., & Hou, K. J. (2018). Ediacaran magmatism in the North Lhasa terrane, Tibet and its tectonic implications. *Precambrian Research*, *307*, 137–154. https://doi.org/10.1016/j.precamres.2018.01.012

Hu, P. Y., Zhai, Q. G., Zhao, G. C., Wang, J., Tang, Y., Wang, H. T., et al. (2018). Early Neoproterozoic (ca. 900 Ma) rift sedimentation and mafic magmatism in the North Lhasa terrane, Tibet: Paleogeographic and tectonic implications. *Lithos*, *320–321*, 403–415. https://doi.org/10.1016/j.lithos.2018.09.036

Hu, X. M., Garzanti, E., Wang, J. G., Huang, W. T., An, W., & Webb, A. (2016). The timing of India-Asia collision onset-Facts, theories, controversies. *Earth-Science Reviews*, *160*, 264–299. https://doi.org/10.1016/j.earscirev.2016.07.014

Iizuka, T., Campbell, I. H., Allen, C. M., Gill, J. B., Maruyama, S., & Makoka, F. (2013). Evolution of the African continental crust as recorded by U–Pb, Lu–Hf and O isotopes in detrital zircons from modern rivers. *Geochimica et Cosmochimica Acta*, *107*, 96–120. https://doi.org/10.1016/j.gca.2012.12.028

Kapp, P., & DeCelles, P. G. (2019). Mesozoic-Cenozoic geological evolution of the Himalayan-Tibetan orogen and working tectonic hypotheses. *American Journal of Science*, *319*(3), 159–254. https://doi.org/10.2475/03.2019.01

Lin, Y. H., Zhang, Z. M., Dong, X., Shen, K., & Lu, X. (2013). Precambrian evolution of the Lhasa terrane, Tibet: Constraint from the zircon U-Pb geochronology of the gneisses. *Precambrian Research*, *237*, 64–77. https://doi.org/10.1016/j.precamres.2013.09.006

Ludwig, K. J. (2003). *ISOPLOT 3.0. Berkeley geochronol* (Vol. 4, p. 70). Center Spec. Publ.

McKenzie, N. R., Smye, A. J., Hegde, V. S., & Stockli, D. F. (2018). Continental growth histories revealed by detrital zircon trace elements: A case study from India. *Geology*, *46*(3), 275–278. https://doi.org/10.1130/g39973.1

Merdith, A. S., Collins, A. S., Williams, S. E., Pisarevsky, S., Foden, J. D., Archibald, D. B., et al. (2017). A full-plate global reconstruction of the Neoproterozoic. *Gondwana Research*, *50*, 84–134. https://doi.org/10.1016/j.gr.2017.04.001

Nance, R. D., Murphy, J. B., & Santosh, M. (2014). The supercontinent cycle: A retrospective essay. *Gondwana Research*, *25*(1), 4–29. https://doi.org/10.1016/j.gr.2012.12.026

Palin, R. M., White, R. W., & Green, E. C. R. (2016). Partial melting of metabasic rocks and the generation of tonalitic–trondhjemitic–granodioritic(TTG) crust in the Archaean: Constraints from phase equilibrium modeling. *Precambrian Research*, *287*, 73–90. https://doi.org/10.1016/j.precamres.2016.11.001

Qian, Q., & Hermann, J. (2013). Partial melting of lower crust at 10-15 kbar: Constraints on adakite and TTG formation. *Contributions to Mineralogy and Petrology*, *165*(6), 1195–1224. https://doi.org/10.1007/s00410-013-0854-9

Ren, M. (2004). Partitioning of Sr, Ba, Rb, Y, and LREE between alkali feldspar and peraluminous silicic magma. *American Mineralogist*, *89*(8–9), 1290–1303. https://doi.org/10.2138/am-2004-8-918

Rubatto, D., Chakraborty, S., & Dasgupta, S. (2013). Timescales of crustal melting in the Higher Himalayan Crystallines (Sikkim, Eastern Himalaya) inferred from trace element-constrained monazite and zircon chronology. *Contributions to Mineralogy and Petrology*, *165*(2), 349–372. https://doi.org/10.1007/s00410-012-0812-y

Rudnick, R. L., & Gao, S. (2014). Composition of the continental crust. In R. L. Rudnick (Ed.), *Treatise on geochemistry*, *The crust* (2nd ed., Vol. 4, pp. 1–51). Elsevier.

Spencer, C. J., Hawkesworth, C., Cawood, P. A., & Dhuime, B. (2013). Not all supercontinents are created equal: Gondwana-Rodinia case study. *Geology*, *41*(7), 795–798. https://doi.org/10.1130/g34520.1

Tang, M., Erdman, M., Eldridge, G., & Lee, C. T. A. (2018). The redox "filter" beneath magmatic orogens and the formation of continental crust. *Science Advances*, *4*(5), eaar4444. https://doi.org/10.1126/sciadv.aar4444

Tang, M., Ji, W. Q., Chu, X., Wu, A. B., & Chen, C. (2020). Reconstructing crustal thickness evolution from europium anomalies in detrital zircons. *Geology*, *49*(1), 76–80. https://doi.org/10.1130/g47745.1

Tang, M., Xu, C., Hao, J. H., & Shen, B. (2021). Orogenic quiescence in Earth's middle age. *Science*, *371*(6530), 728–731. https://doi.org/10.1126/science.abf1876

Triantafyllou, A., Ducea, M. N., Jepson, G., Hernández-Montenegro, J. D., Bisch, A., & Ganne, J. (2023). Europium anomalies in detrital zircons record major transitions in Earth geodynamics at 2.5 Ga and 0.9 Ga. *Geology*, *51*(2), 141–145. https://doi.org/10.1130/g050720.1

Wang, C., Mitchell, R. N., Murphy, J. B., Peng, P., & Spencer, C. J. (2021). The role of megacontinents in the supercontinent cycle. *Geology*, *49*(4), 402–406. https://doi.org/10.1130/g47988.1

19448007, 2023, 5, Downloaded from https://agupubs.onlinelibrary.wiley.com/doi/10.1029/2023GL102979 by University of Hong Kong, Wiley Online Library on [18/09/2023]. See the Terms and Conditions (https://onlinelibrary.wiley.com/terms-and-conditions) on Wiley Online Library for rules of use; OA articles are governed by the applicable Creative Commons License

Wang, Q., Chung, S. L., Li, X. H., Wyman, D., Li, Z. X., Sun, W. D., et al. (2012). Crustal melting and flow beneath northern Tibet: Evidence from MidMiocene to Quaternary strongly peraluminous rhyolites in the southern Kunlun Range. *Journal of Petrology*, *53*(12), 2523–2566. https://doi.org/10.1093/petrology/egs058

Wang, Q., Zhu, D. C., Zhao, Z. D., Liu, S. A., Chung, S. L., Li, S. M., et al. (2014). Origin of the ca. 90 Ma magnesia-rich volcanic rocks in SE Nyima, central Tibet: Products of lithospheric delamination beneath the Lhasa-Qiangtang collision zone. *Lithos*, *198–199*, 24–37. https://doi.org/10.1016/j.lithos.2014.03.019

Wang, R., Weinbergc, R. F., Collins, W. J., Richards, J. P., & Zhu, D. C. (2018). Origin of postcollisional magmas and formation of porphyry Cu deposits in southern Tibet. *Earth-Science Reviews*, *181*, 122–143. https://doi.org/10.1016/j.earscirev.2018.02.019

Wang, W., Cawood, P. A., Pandit, M. K., Zhao, J. H., & Zheng, J. P. (2019). No collision between Eastern and Western Gondwana at their northern extent. *Geology*, *47*(4), 308–312. https://doi.org/10.1130/g45745.1

Wu, Y., Ma, X. X., Zhang, Z. P., Jiao, S. W., Duan, K., Dong, H., et al. (2016). Geochemical features of the Nyainqentanglha Group in the western Lhasa terrane, western Tibet and their tectonic significance. *Acta Geologica Sinica*, *90*, 3081–3098. [in Chinese with English abstract].

Zhao, G. C., Wang, Y. J., Huang, B. C., Dong, Y. P., Li, S. Z., Zhang, G. W., & Yu, S. (2018). Geological reconstructions of the East Asian blocks: From the breakup of Rodinia to the assembly of Pangea. *Earth-Science Reviews*, *186*, 262–286. https://doi.org/10.1016/j.earscirev.2018.10.003

Zhao, S. Y., Yang, A. Y., Langmuir, C. H., & Zhao, T. P. (2022). Oxidized primary arc magmas: Constraints from Cu/Zr systematics in global arc volcanics. *Science Advances*, *8*(12), eabk0718. https://doi.org/10.1126/sciadv.abk0718

Zhao, Z. B., Li, C., & Ma, X. X. (2021). How does the elevation changing response to crustal thickening process in the central Tibetan Plateau since 120 Ma? *China Geology*, *4*(1), 32–43. https://doi.org/10.31035/cg2021013

Zhu, D. C., Mo, X. X., Zhao, Z. D., Niu, Y. L., Wang, L. Q., Chu, Q. H., et al. (2010). Presence of Permian extension- and arc-type magmatism in southern Tibet: Paleogeographic implications. *The Geological Society of America Bulletin*, *122*(7–8), 979–993. https://doi.org/10.1130/b30062.1

Zhu, D. C., Wang, Q., Cawood, P. A., Zhao, Z. D., & Mo, X. X. (2017). Raising the Gangdese Mountains in southern Tibet. *Journal of Geophysical Research: Solid Earth*, *122*(1), 214–223. https://doi.org/10.1002/2016jb013508

Zhu, D. C., Wang, Q., Weinberg, R. F., Cawood, P. A., Chung, S. L., Zheng, Y. F., et al. (2022). Interplay between oceanic subduction and continental collision in building continental crust. *Nature Communications*, *13*(1), 7141. https://doi.org/10.1038/s41467-022-34826-0

Zhu, D. C., Wang, Q., Zhao, Z. D., Chung, S. L., Cawood, P. A., Niu, Y. L., et al. (2015). Magmatic record of India-Asia collision. *Scientific Reports*, *5*(1), 14289. https://doi.org/10.1038/srep14289

Zhu, D. C., Zhao, Z. D., Niu, Y., Dilek, Y., & Mo, X. X. (2011). Lhasa terrane in southern Tibet came from Australia. *Geology*, *39*(8), 727–730. https://doi.org/10.1130/g31895.1

Zhu, Z. Y., Campbell, I. H., Allen, C. M., Brocks, J. J., & Chen, B. (2022). The temporal distribution of Earth's supermountains and their potential link to the rise of atmospheric oxygen and biological evolution. *Earth and Planetary Science Letters*, *580*, 117391. https://doi.org/10.1016/j.epsl.2022.117391

Zhu, Z. Y., Campbell, I. H., Allen, C. M., & Burnham, A. D. (2020). S-type granites: Their origin and distribution through time as determined from detrital zircons. *Earth and Planetary Science Letters*, *536*, 116140. https://doi.org/10.1016/j.epsl.2020.116140

Zoleikhaei, Y., Mulder, J. A., & Cawood, P. A. (2021). Integrated detrital rutile and zircon provenance reveals multiple sources for Cambrian sandstones in North Gondwana. *Earth-Science Reviews*, *213*, 103462. https://doi.org/10.1016/j.earscirev.2020.103462

Zoleikhaei, Y., Mulder, J. A., & Cawood, P. A. (2022). Evaluating sediment recycling through combining inherited petrogenic and acquired sedimentary features of multiple detrital minerals. *Basin Research*, *34*(3), 1055–1083. https://doi.org/10.1111/bre.12650

References From the Supporting Information

Armandolaa, S., Barhama, M., Reddy, S. M., Clark, C., & Spinks, S. (2018). Footprint of a large intracontinental rifting event: Coupled detrital zircon geochronology and geochemistry from the Mesoproterozoic Collier Basin, Western Australia. *Precambrian Research*, *318*, 156–169. https://doi.org/10.1016/j.precamres.2018.09.006

Avigad, D., Gerdes, A., Morag, N., & Bechstädt, T. (2012). Coupled U–Pb–Hf of detrital zircons of Cambrian sandstones from Morocco and Sardinia: Implications for provenance and Precambrian crustal evolution of North Africa. *Gondwana Research*, *21*(2–3), 690–703. https://doi.org/10.1016/j.gr.2011.06.005

Avigad, D., Weissbrod, T., Gerdes, A., Zlatkin, O., Ireland, T. R., & Morag, N. (2015). The detrital zircon U-Pb-Hf fingerprint of the northern Arabian-Nubian Shield as reflected by a Late Ediacaran arkosic wedge (Zenifim Formation; subsurface Israel). *Precambrian Research*, *266*, 1–11. https://doi.org/10.1016/j.precamres.2015.04.011

Balica, C., Ducea, M. N., Gehrels, G. E., Kirk, J., Roban, R. D., Luffi, P., et al. (2020). A zircon petrochronologic view on granitoids and continental evolution. *Earth and Planetary Science Letters*, *531*, 116005. https://doi.org/10.1016/j.epsl.2019.116005

Barham, M., Kirkland, C. L., Reynolds, S., O'Leary, M. J., Evans, N. J., Allen, H., et al. (2016). The answers are blowin' in the wind: Ultra-distal ashfall zircons, indicators of Cretaceous super-eruptions in eastern Gondwana. *Geology*, *44*(8), 643–646. https://doi.org/10.1130/g38000.1

Bicca, M. M., Jelinek, A. R., Philipp, R. P., Lana, C. D. C., & Alkmim, A. R. (2018). Precambrian-Cambrian provenance of Matinde Formation, Karoo Supergroup, northwestern Mozambique, constrained from detrital zircon U-Pb age and Lu-Hf isotope data. *Journal of African Earth Sciences*, *138*, 42–57. https://doi.org/10.1016/j.jafrearsci.2017.10.013

Cao, H. W., Huang, Y., Li, G. M., Zhang, L. K., Wu, J. Y., Dong, L., et al. (2018). Late Triassic sedimentary records in the northern Tethyan Himalaya: Tectonic link with Greater India. *Geoscience Frontiers*, *9*(1), 273–291. https://doi.org/10.1016/j.gsf.2017.04.001

Cawood, P. A., & Nemchin, A. A. (2000). Provenance record of a rift basin: U/Pb ages of detrital zircons from the Perth Basin, Western Australia. *Sedimentary Geology*, *134*(3–4), 209–234. https://doi.org/10.1016/s0037-0738(00)00044-0

Chen, L. R., Xu, W. C., Zhang, H. F., Zhao, P. L., Guo, J. L., Luo, B. J., et al. (2019). Origin and early evolution of the Lhasa Terrane, south Tibet: Constraints from the Bomi Gneiss Complex. *Precambrian Research*, *331*, 105360. https://doi.org/10.1016/j.precamres.2019.105360

Chen, Y. F., Zhang, Z. M., Chen, X. H., Palin, R. M., Tian, Z. L., Shao, Z. G., et al. (2022). Neoproterozoic and early Paleozoic magmatism in the eastern Lhasa terrane: Implications for Andean-type orogeny along the northern margin of Rodinia and Gondwana. *Precambrian Research*, *369*, 106520. https://doi.org/10.1016/j.precamres.2021.106520

Chu, N. C., Taylor, R. N., Chavagnac, V., Nesbitt, R. W., Boella, R. M., Mitton, J. A., et al. (2002). Hf isotope ratio analysis using multi-collector inductively coupled plasma mass spectrometry: An evaluation of isobaric interference corrections. *Journal of Analytical Atomic Spectrometry*, *17*(12), 1567–1574. https://doi.org/10.1039/b206707b

Dong, X., Zhang, Z. M., Wang, J. L., Zhao, G. C., Liu, F., Wang, W., & Yu, F. (2009). Provenance and formation age of the Nyingchi Group in the southern Lhasa terrane, Tibetan Plateau:Petrology and zircon U-Pb geochronology. *Acta Petrologica Sinica*, *25*, 1678–1694. [in Chinese with English abstract].

Dong, X., Zhang, Z. M., Santosh, M., Wang, W., Yu, F., & Liu, F. (2011a). Late Neoproterozoic thermal events in the northern Lhasa terrane, south Tibet: Zircon chronology and tectonic implications. *Journal of Geodynamics*, *52*(5), 389–405. https://doi.org/10.1016/j.jog.2011.05.002

Dong, C. Y., Li, C., Wan, Y. S., Wang, W., Wu, Y. W., Xie, H. Q., & Liu, D. Y. (2011b). Detrital zircon age model of Ordovician Wenquan quartzite south of Lungmuco-Shuanghu Suture in the Qiangtang area, Tibet: Constraint on tectonic affinity and source regions. *Science China Earth Sciences*, *54*(7), 1034–1042. https://doi.org/10.1007/s11430-010-4166-x

Dong, X., Zhang, Z. M., Niu, Y. L., Tian, Z. L., & Zhang, L. L. (2020). Reworked Precambrian metamorphic basement of the Lhasa terrane, southern Tibet: Zircon/titanite U-Pb geochronology, Hf isotope and geochemistry. *Precambrian Research*, *336*, 105496. https://doi.org/10.1016/j.precamres.2019.105496

Elhlou, S., Belousova, E., Griffin, W. L., Pearson, N. J., & O'Reilly, S. Y. (2006). Trace element and isotopic composition of GJ-red zircon standard by laser ablation. *Geochimica et Cosmochimica Acta*, *70*(18), A158. https://doi.org/10.1016/j.gca.2006.06.1383

Hiess, J., Yi, K., Woodhead, J., Ireland, T., & Rattenbury, M. (2015). Gondwana margin evolution from zircon REE, O and Hf signatures of Western Province gneisses, Zealandia. *Geological Society, London, Special Publications*, *389*(1), 323–353. https://doi.org/10.1144/SP389.10

Hou, K. J., Li, Y. H., Zou, T. R., Qu, X. M., Shi, Y. R., & Xie, G. Q. (2007). Laser ablation-MC-ICP-MS technique for Hf isotope microanalysis of zircon and its geological applications. *Acta Petrologica Sinica*, *23*, 2595–2604. [in Chinese with English abstract].

Hou, K. J., Li, Y. H., & Tian, Y. Y. (2009). In situ U-Pb zircon dating using laser ablation-multi ion couting-ICP-MS. *Mineral Deposits*, *28*, 481–492. [in Chinese with English abstract].

Hu, P. Y., Li, C., Wang, M., Xie, C. M., & Wu, Y. W. (2013). Cambrian volcanism in the Lhasa terrane, southern Tibet: Record of an early Paleozoic Andean-type magmatic arc along the Gondwana proto-Tethyan margin. *Journal of Asian Earth Sciences*, *77*, 91–107. https://doi.org/10.1016/j.jseaes.2013.08.015

Hu, P. Y., Zhai, Q. G., Tang, Y., Wang, J., & Wang, H. T. (2016). Early Neoproterozoic meta-gabbro (~925 Ma) from the Lhasa terrane, Tibetan Plateau and its geological significance. *Chinese Science Bulletin*, *61*(19), 2176–2186. [in Chinese with English abstract]. https://doi.org/10.1360/n972016-00143

Hu, P. Y., Zhai, Q. G., Wang, J., Tang, Y., Wang, H. T., & Hou, K. J. (2018b). Precambrian origin of the North Lhasa terrane, Tibetan Plateau: Constraint from early Cryogenian back-arc magmatism. *Precambrian Research*, *313*, 51–67. https://doi.org/10.1016/j.precamres.2018.05.014

Hu, P. Y., Zhai, Q. G., Wang, J., Tang, Y., Wang, H. T., Zhu, Z. C., & Wu, H. (2018c). Middle Neoproterozoic (ca. 760 Ma) arc and back-arc system in the North Lhasa terrane, Tibet, inferred from coeval N-MORB- and arc-type gabbros. *Precambrian Research*, *316*, 275–290. https://doi.org/10.1016/j.precamres.2018.08.022

Hu, P. Y., Zhai, Q. G., Wang, J., Tang, Y., Wang, H. T., & Hou, K. J. (2018d). Ediacaran magmatism in the North Lhasa terrane, Tibet and its tectonic implications. *Precambrian Research*, *307*, 137–154. https://doi.org/10.1016/j.precamres.2018.01.012

Hu, P. Y., Zhai, Q. G., Zhao, G. C., Wang, J., Tang, Y., Zhu, Z. C., & Wu, H. (2019a). The North Lhasa terrane in Tibet was attached with the Gondwana before it was drafted away in Jurassic: Evidence from detrital zircon studies. *Journal of Asian Earth Sciences*, *185*, 104055. https://doi.org/10.1016/j.jseaes.2019.104055

Hu, P. Y., Zhai, Q. G., Zhao, G. C., Wang, J., Tang, Y., Wang, H. T., et al. (2019b). Late Cryogenian magmatic activity in the North Lhasa terrane, Tibet: Implication of slab break-off process. *Gondwana Research*, *71*, 129–149. https://doi.org/10.1016/j.gr.2019.02.005

Hu, P. Y., Zhai, Q. G., Cawood, P. A., Zhao, G. C., Wang, J., Tang, Y., et al. (2021). Cambrian magmatic flare-up, central Tibet: Magma mixing in proto-Tethyan arc along north Gondwanan margin. *GSA Bulletin*, *133*(9–10), 2171–2188. https://doi.org/10.1130/b35859.1

Hu, P. Y., Zhai, Q. G., Cawood, P. A., Zhao, G. C., Wang, J., Tang, Y., et al. (2022). Middle Neoproterozoic (ca. 700 Ma) tectonothermal events in the Lhasa terrane, Tibet: Implications for paleogeography. *Gondwana Research*, *104*, 252–264. https://doi.org/10.1016/j.gr.2021.01.014

Iizuka, T., Komiya, T., Rino, S., Maruyama, S., & Hirata, T. (2010). Detrital zircon evidence for Hf isotopic evolution of granitoid crust and continental growth. *Geochimica et Cosmochimica Acta*, *74*(8), 2450–2472. https://doi.org/10.1016/j.gca.2010.01.023

Iizuka, T., Campbell, I. H., Allen, C. M., Gill, J. B., Maruyama, S., & Makoka, F. (2013). Evolution of the African continental crust as recorded by U-Pb, Lu-Hf and O isotopes in detrital zircons from modern rivers. *Geochimica et Cosmochimica Acta*, *107*, 96–120. https://doi.org/10.1016/j.gca.2012.12.028

Jackson, S. E., Pearson, N. J., Griffin, W. L., & Belousova, E. A. (2004). The application of laser ablation-inductively coupled plasma-mass spectrometry to in situ U-Pb zircon geochronology. *Chemical Geology*, *211*(1–2), 47–69. https://doi.org/10.1016/j.chemgeo.2004.06.017

Kolodner, K., Avigad, A., Mcwilliams, M., Wooden, J. L., Weissbrod, T., & Feinstein, S. (2006). Provenance of north Gondwana Cambrian-Ordovician sandstone: U-Pb SHRIMP dating of detrital zircons from Israel and Jordan. *Geological Magazine*, *143*(3), 367–391. https://doi.org/10.1017/s0016756805001640

Leier, A. L., Kapp, P., Gehrels, G. E., & DeCelles, P. G. (2007). Detrital zircon geochronology of Carboniferous-Cretaceous strata in the Lhasa terrane, southern Tibet. *Basin Research*, *19*(3), 361–378. https://doi.org/10.1111/j.1365-2117.2007.00330.x

Liu, Y. S., Gao, S., Hu, Z. C., Gao, C. G., Zong, K. Q., & Wang, D. B. (2010). Continental and oceanic crust recycling-induced melt-peridotite interactions in the Trans-North China Orogen: U-Pb dating, Hf isotopes and trace elements in zircons from mantle xenoliths. *Journal of Petrology*, *51*(1–2), 537–571. https://doi.org/10.1093/petrology/egp082

Lloyd, J., Collins, A. S., Payne, J. L., Glorie, S., Holford, S., & Reid, A. J. (2016). Tracking the Cretaceous transcontinental Ceduna River through Australia: The hafnium isotope record of detrital zircons from offshore southern Australia. *Geoscience Frontiers*, *7*(2), 237–244. https://doi.org/10.1016/j.gsf.2015.06.001

McKenzie, N. R., Hughes, N. C., Myrow, P. M., Xiao, S. H., & Sharma, M. (2011). Correlation of Precambrian–Cambrian sedimentary successions across northern India and the utility of isotopic signatures of Himalayan lithotectonic zones. *Earth and Planetary Science Letters*, *312*(3–4), 471–483. https://doi.org/10.1016/j.epsl.2011.10.027

McKenzie, N. R., Hughes, N. C., Myrow, P. M., Banerjee, D. M., Deb, M., & Planavsky, N. J. (2013). New age constraints for the Proterozoic Aravalli-Delhi successions of India and their implications. *Precambrian Research*, *238*, 120–128. https://doi.org/10.1016/j.precamres.2013.10.006

McKenzie, N. R., Smye, A. J., Hegde, V. S., & Stockli, D. F. (2018). Continental growth histories revealed by detrital zircon trace elements: A case study from India. *Geology*, *46*(3), 275–278. https://doi.org/10.1130/g39973.1

Meinhold, G., Morton, A. C., Fanning, C. M., Frei, D., Howard, J. P., Phillips, R. J., et al. (2011). Evidence from detrital zircons for recycling of Mesoproterozoic and Neoproterozoic crust recorded in Paleozoic and Mesozoic sandstones of southern Libya. *Earth and Planetary Science Letters*, *312*(1–2), 164–175. https://doi.org/10.1016/j.epsl.2011.09.056

Meinhold, G., Morton, A. C., & Avigad, D. (2013). New insights into peri-Gondwana paleogeography and the Gondwana super-fan system from detrital zircon U-Pb ages. *Gondwana Research*, *23*(2), 661–665. https://doi.org/10.1016/j.gr.2012.05.003

19448007, 2023, 5, Downloaded from https://agupubs.onlinelibrary.wiley.com/doi/10.1029/2023GL102979 by University of Hong Kong, Wiley Online Library on [18/09/2023]. See the Terms and Conditions (https://onlinelibrary.wiley.com/terms-and-conditions) on Wiley Online Library for rules of use; OA articles are governed by the applicable Creative Commons License

Olierook, H. K. H., Barham, M., Fitzsimons, I. C. W., Timms, N. E., Jiang, Q., Evans, N. J., & McDonald, B. J. (2019). Tectonic controls on sediment provenance evolution in rift basins: Detrital zircon U-Pb and Hf isotope analysis from the Perth Basin, Western Australia. *Gondwana Research*, *66*, 126–142. https://doi.org/10.1016/j.gr.2018.11.002

O'Neill, H. S. C. (2016). The smoothness and shapes of chondrite-normalized rare Earth element patterns in basalts. *Journal of Petrology*, *57*(8), 1463–1508. https://doi.org/10.1093/petrology/egw047

Purdy, D. J., Cross, A. J., Brown, D. D., Carr, P. A., & Armstrong, R. A. (2016). New constraints on the origin and evolution of the Thomson Orogen and links with central Australia from isotopic studies of detrital zircons. *Gondwana Research*, *39*, 41–56. https://doi.org/10.1016/j.gr.2016.06.010

Sláma, J., Kosler, J., Condon, D. J., Crowley, J. L., Gerdes, A., Hanchar, J. M., et al. (2008). Plesovice zircon — A new natural reference material for U-Pb and Hf isotopic microanalysis. *Chemical Geology*, *249*(1–2), 1–35. https://doi.org/10.1016/j.chemgeo.2007.11.005

Tang, M., Chu, X., Hao, J. H., & Shen, B. (2021). Orogenic quiescence in Earth's middle age. *Science*, *371*(6530), 728–731. https://doi.org/10.1126/science.abf1876

Thomas, R. J., Jacobs, J., Horstwood, M. S. A., Ueda, K., Bingen, B., & Matola, R. (2010). The Mecubúri and Alto Benfica Groups, NE Mozambique: Aids to unravelling ca. 1 and 0.5 Ga events in the East African Orogen. *Precambrian Research*, *178*(1–4), 72–90. https://doi.org/10.1016/j.precamres.2010.01.010

Turner, C. C., Meert, J. G., Pandit, M. K., & Kamenov, G. D. (2014). A detrital zircon U–Pb and Hf isotopic transect across the Son Valley sector of the Vindhyan Basin, India: Implications for basin evolution and paleogeography. *Gondwana Research*, *26*(1), 348–364. https://doi.org/10.1016/j.gr.2013.07.009

Veevers, J. J., Saeed, A., Belousova, E. A., & Griffin, W. L. (2005). U-Pb ages and source composition by Hf-isotope and trace-element analysis of detrital zircons in Permian sandstone and modern sand from southwestern Australia and a review of the paleogeographical and denudational history of the Yilgarn Craton. *Earth-Science Reviews*, *68*(3–4), 245–279. https://doi.org/10.1016/j.earscirev.2004.05.005

Wang, Q., Zhu, D. C., Cawood, P. A., Chung, S. L., & Zhao, Z. D. (2021). Resolving the paleogeographic puzzle of the Lhasa Terrane in southern Tibet. *Geophysical Research Letters*, *48*(15), e2021GL094236. https://doi.org/10.1029/2021gl094236

Wiedenbeck, M., Hanchar, J. M., Peck, W. H., Sylvester, P., Valley, J., Whitehouse, M., et al. (2004). Further characterization of the 91500 zircon crystal. *Geostandards and Geoanalytical Research*, *28*(1), 9–39. https://doi.org/10.1111/j.1751-908x.2004.tb01041.x

Wu, F. Y., Yang, Y. H., Xie, L. W., Yang, J. H., & Ping, C. (2006). Hf isotopic compositions of the standard zircons and baddeleyites used in U-Pb geochronology. *Chemical Geology*, *234*(1–2), 105–126. https://doi.org/10.1016/j.chemgeo.2006.05.003

Xu, W. C., Zhang, H. F., Harris, N., Guo, L., Pan, F. B., & Wang, S. (2013). Geochronology and geochemistry of Mesoproterozoic granitoids in the Lhasa terrane, south Tibet: Implications for the early evolution of Lhasa terrane. *Precambrian Research*, *236*, 46–58. https://doi.org/10.1016/j.precamres.2013.07.016

Zeng, Y. C., Chen, Q., Xu, J. F., Chen, J. L., Huang, F., Yu, H. X., & Zhao, P. P. (2018). Petrogenesis and geodynamic significance of Neoproterozoic (~925 Ma) high-Fe-Ti gabbros of the RenTso ophiolite, Lhasa Terrane, central Tibet. *Lithos*, *300–301*, 250–260. https://doi.org/10.1016/j.lithos.2017.11.025

Zhang, Z. M., Dong, X., Liu, F., Lin, Y., Yan, R., He, Z., & Santosh, M. (2012). The making of Gondwana: Discovery of 650 Ma HP granulites from North Lhasa, Tibet. *Precambrian Research*, *212*, 107–116. https://doi.org/10.1016/j.precamres.2012.04.018

Zhou, X., Zheng, J. P., Li, Y. B., Griffin, W. L., Xiong, Q., Moghadam, H. S., & O'Reilly, S. Y. (2019). Neoproterozoic sedimentary rocks track the location of the Lhasa Block during the Rodinia breakup. *Precambrian Research*, *320*, 63–77. https://doi.org/10.1016/j.precamres.2018.10.005

Zhu, D. C., Zhao, Z. D., Niu, Y. L., Dilek, Y., Wang, Q., Ji, W. H., et al. (2012). Cambrian bimodal volcanism in the Lhasa terrane, southern Tibet: Record of an early Paleozoic Andean-type magmatic arc in the Australian proto-Tethyan margin. *Chemical Geology*, *328*, 290–308. https://doi.org/10.1016/j.chemgeo.2011.12.024

19448007, 2023, 5, Downloaded from https://agupubs.onlinelibrary.wiley.com/doi/10.1029/2023GL102979 by University of Hong Kong, Wiley Online Library on [18/09/2023]. See the Terms and Conditions (https://onlinelibrary.wiley.com/terms-and-conditions) on Wiley Online Library for rules of use; OA articles are governed by the applicable Creative Commons License